

**Keywords:** spiroid gear; worm; face wheel; gear lubrication; oil film

Aleksander MAZURKOW,<sup>1</sup> Wojciech HOMIK<sup>2\*</sup>

## OPERATION OF A SPIROID GEAR UNDER ELASTOHYDRODYNAMIC LUBRICATION CONDITIONS

**Summary.** Spiroid gears are used in the drive systems of various types of vehicles and devices. They are characterised by small overall dimensions and significant rotational speed reduction while maintaining the high positioning accuracy of the driven device. Spiroid gears require a lot of lubrication with oils, which separate the mating parts. In the case of spiroid gears, they separate the face wheel teeth and the worm thread. The resulting oil film reduces the coefficient of friction and lowers the temperature of the mating surfaces. The modelling of toothed rim lubrication is a complex problem. To separate the surface of the face wheel mating and the worm, one needs to consider the phenomena of fluid mechanics, heat transfer and tooth deformation. The formation of an elastohydrodynamic oil film of an appropriate height is determined by the type of oil, the mechanical properties of the worm and face wheel materials, relative speed, load and the geometry of the mating surfaces. The issues described in this paper significantly affect the correct operation of gears and have not yet been fully understood for spiroid gears. This paper presents the results of a study on the properties of the elastohydrodynamic oil film and describes its characteristics, with the unknown quantity being the rotational speed of the input shaft that ensures that the oil film separates the mating toothed rims. The calculation results were compared with those of other researchers. The obtained design recommendations can help designers improve the durability and reliability of spiroid gears.

### 1. INTRODUCTION

Structures such as gears [1-3] require oil lubrication of the mating and moving surfaces of the toothed rims. The profiles of these surfaces can be flat, convex or concave. The mating surfaces form slots which converge to some extent (Fig. 1).

Oil is forced into the tapering part of a slot as a result of viscosity shear stability. When the oil flows through the tapering slot, the oil pressure increases. The hydrodynamic buoyancy force balancing the load depends on the shape and dimensions of the surfaces, the properties of the materials from which these surfaces are made and the properties of the oil used.

In the case of a Newtonian fluid (Fig. 2), the relation between tangential stresses  $\tau_{xy}$  and oil flow velocity gradient  $\frac{dv_x}{dy}$  is represented by the equation:

$$\tau_{xy} = \eta \cdot \frac{dv_x}{dy} \quad (1)$$

where:  $\eta$  is the dynamic oil viscosity.

---

<sup>1</sup> Rzeszów University of Technology; Powstańców Warszawy 12, 35-959 Rzeszów, Poland; e-mail: [almaz@prz.edu.pl](mailto:almaz@prz.edu.pl); [orcid.org/0000-0003-1719-991X](https://orcid.org/0000-0003-1719-991X)

<sup>2</sup> Rzeszów University of Technology; Powstańców Warszawy 12, 35-959 Rzeszów, Poland; e-mail: [whomik@prz.edu.pl](mailto:whomik@prz.edu.pl); [orcid.org/0000-0001-7843-7761](https://orcid.org/0000-0001-7843-7761)

\* Corresponding author. E-mail: [whomik@prz.edu.pl](mailto:whomik@prz.edu.pl)

If there is a large increase in oil pressure, the elastic deformation of the mating surfaces of the face wheel and the worm is also likely to occur. To ensure continuity of flow, it is also important to ensure a sufficiently high oil flow rate. One effect of the discussed elastohydrodynamic lubrication method is a reduction in the friction coefficient between the mating surfaces of the toothed rims. When this lubrication method is used, it is also important to ensure a continuous flow of oil.

The authors carried out bench tests [4], focusing on problems with the lubrication of spiroid gears. This turned out to be a complex problem. The fundamental (specific) problem is posed by the measurement of the oil film parameters, such as temperature, pressure or film thickness. The obtained measurement results do not give full information about the conditions ensuring the separation of the mating surfaces of toothed rims with an oil film.

Therefore, the authors used theoretical models to analyse and determine the influences of gear loading torque, the rotational speed of the input shaft and oil viscosity grade on the possibility of separating the mating surfaces of the toothed rims with an oil film that guarantees fluid friction. The authors believe that this will ensure an appropriately high durability and reliability of spiroid gears [5, 6].

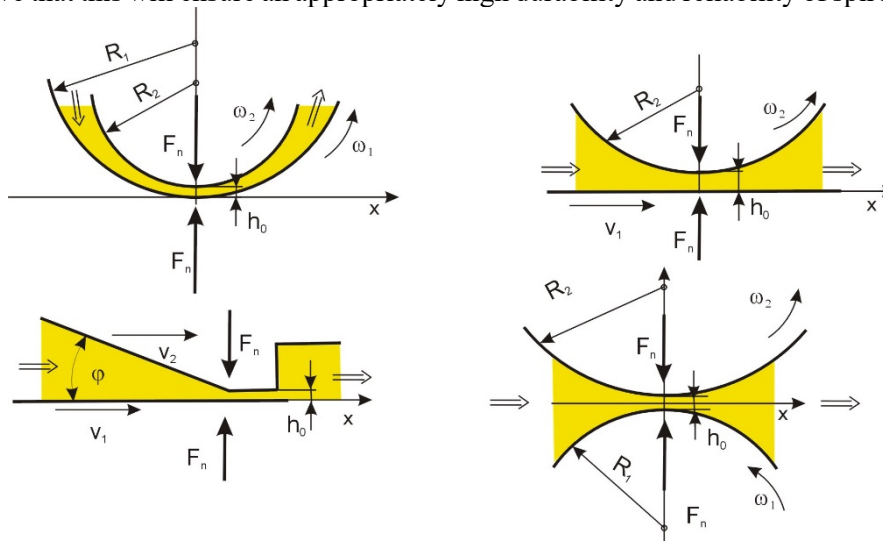


Fig. 1. Typical shapes of sliding surface profiles:  $R_{1,2,L}$  – curvature radius of the mating surfaces,  $F_n$ – load,  $v_{1,2}$  – linear speed,  $\omega_{1,2}$  – angular velocity,  $h_0$ – minimum oil film height

The construction of a gear (Fig. 3) consists of two basic parts [7-9]: a toothed face wheel and a worm. Spiroid gears are used in the drive systems of various types of machines in the aviation and automotive industry, where significant speed reduction is required with small overall dimensions while the driven device’s positioning accuracy remains high [10-13].

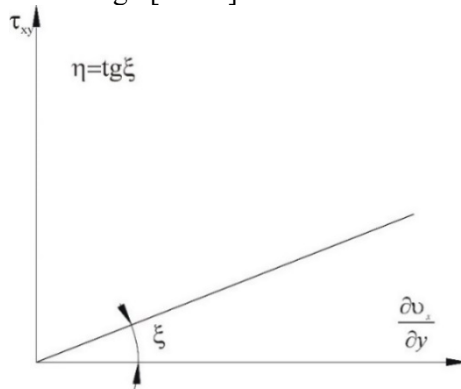


Fig. 2. Newtonian fluid model:  $\xi$ – angle characterising the viscosity function

Numerical calculations were carried out using appropriate physical and mathematical models of the elastohydrodynamic oil film. Their solution provided the authors with the static characteristics of the oil film.

This paper presents the results of a study on the effects of selected parameters on the rotational speed enabling the generation of the minimum oil film height that guarantees separation of the mating surfaces. These parameters include load, oil viscosity grade, mechanical properties of the worm and face wheel materials and mesh geometry.

The presented method of calculating the elastohydrodynamic oil film can be useful in determining the performance characteristics of gears and improving their durability and reliability. An analysis of the available knowledge of spiroid gears showed that this kind of research has not been conducted and its results have not been published.

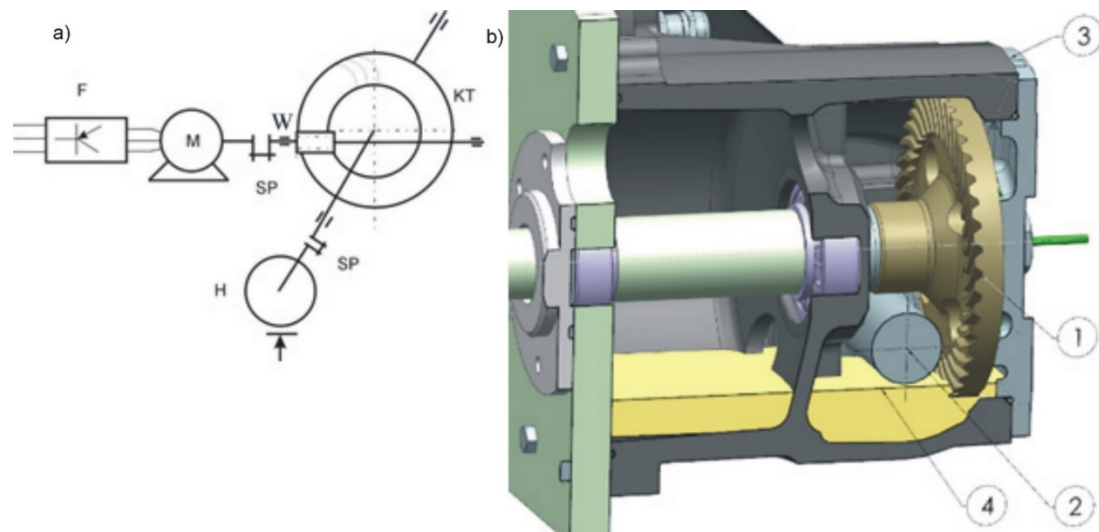


Fig. 3. a) Test bench structure: F – inverter, M – motor, SP – clutch, W – worm, KT – face wheel, H – brake, b) spiroid gear construction: body (1), worm (2), face wheel (3), level of oil lubricating toothed rims (4)

## 2. THERMOPHYSICAL PROPERTIES OF OIL

The basic quantities characterising the thermophysical properties of oils [14] operating under elastohydrodynamic lubrication conditions are dynamic viscosity  $\eta(p, T)$  and density  $\rho(p, T)$ .

Viscosity is the measure of internal friction. As shown by the results of measurements [15], the dynamic viscosity of oils significantly depends on pressure  $p$  and temperature  $T$  (Fig. 4).

An analysis of the viscosity function  $\eta(p, T)$  shows that an increase in temperature results in a decrease in dynamic viscosity. In contrast, an increase in pressure results in an increase in dynamic viscosity.

Various mathematical models are used to describe the viscosity function. The following relations summarize some functions describing the thermophysical properties of oils [16-21]:

$$\eta = \eta_0 \cdot e^{\alpha_p \cdot p}, \quad (2)$$

$$\eta = \eta_0 \cdot e^{(\alpha_p \cdot p - \beta_T (T - T_0))}, \quad (3)$$

$$\ln \frac{\eta}{A} = \ln \frac{\eta_0}{A} \cdot \left( \frac{p}{2000} + 1 \right)^{D + E \cdot \ln \frac{\eta_0}{A}}, \quad (4)$$

where:  $p$  – oil film pressure,  $\eta_0$  – dynamic viscosity of oil measured at ambient temperature and pressure,  $A$ ,  $D$ ,  $E$ ,  $\alpha_p$  – coefficient of the effect of pressure on dynamic viscosity,  $\beta_T$  – coefficient of the effect of temperature on dynamic viscosity. Oil density, as a function of pressure and temperature  $\rho(p, T)$ , can be described (Fig. 5) by the following equations [22]:

$$\rho(T) = \rho_0 + a_\rho \cdot T + b_\rho \cdot T^2, \quad (5)$$

$$\rho(p) = \rho_0 \left( 1 + \frac{5.921 \cdot 10^{-10} p}{1 + 5.921 \cdot 10^{-9} p} \right), \quad (6)$$

where:  $T$  – temperature,  $\rho_0$  – oil density measured at ambient temperature and pressure,  $a_\rho, b_\rho$  – coefficients of the effect of temperature on oil density.

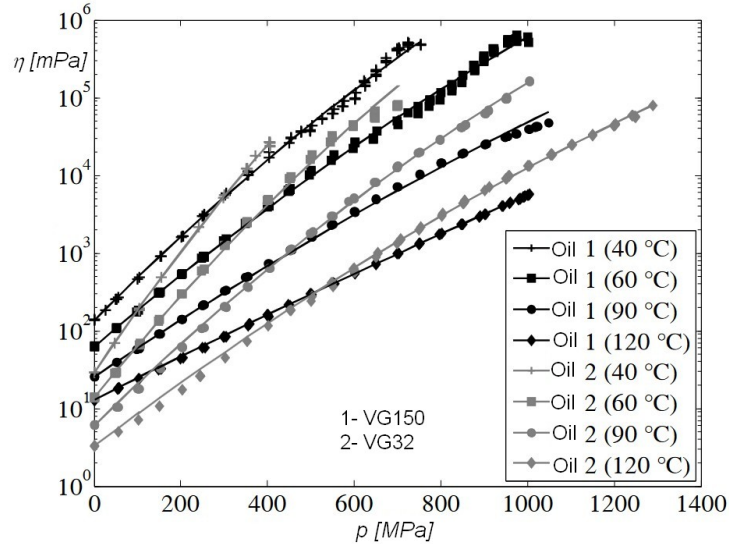


Fig. 4. Dynamic viscosity of VG 32 and VG 150 oils as a function of pressure and temperature [15]

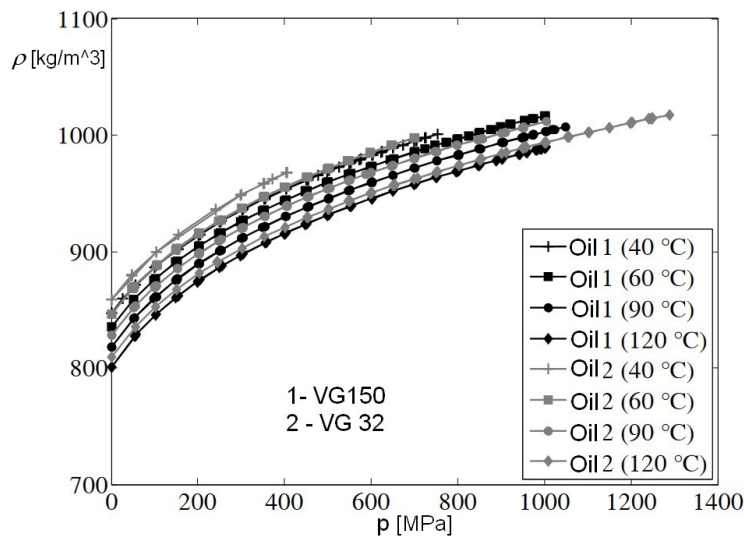


Fig. 5. Density of VG 32 and VG 150 oils as a function of pressure and temperature [15]

### 3. ASSUMPTIONS FOR THE ELASTOHYDRODYNAMIC LUBRICATION MODEL

The development of mathematical models of the elastohydrodynamic oil film (Fig. 6) was based on the following assumptions [17, 18, 23]:

- deformations of the mating surfaces are elastic,
- equations of oil viscosity and density functions take into account the effects of pressure and temperature,

- oil flow is laminar and steady,
- inertia forces during oil flow are negligible,
- oil flow in the tooth space is unidirectional (in the direction of the tooth space convergence), and other oil flow directions are negligibly small,
- oil film temperature is constant,
- a Newtonian fluid model is adopted,
- there is no slippage on the boundary surfaces,
- the velocity of the boundary layer of the oil and the tooth surface are equal.

#### 4. TOOTH SPACE PRESSURE DISTRIBUTION EQUATION

The principle of conservation of momentum for fluids is represented by the Navier-Stokes equation:

$$\frac{d\bar{v}}{dt} = \bar{F}_m - \frac{1}{\rho} \text{grad } p + \frac{1}{3} \cdot v \cdot \text{grad } \text{div} \bar{v} + v \cdot \Delta \bar{v}, \quad (7)$$

where:  $v$  – kinematic oil viscosity,  $\bar{F}_m$  – body force.

Based on the assumptions outlined in Section 3, Equation (7) takes the following form:

$$0 = \frac{1}{\rho} \cdot \left( -\frac{\partial p}{\partial x} + \eta \cdot \frac{\partial^2 v_x}{\partial x^2} \right). \quad (8)$$

Equation (8) is satisfied when the expression in brackets is zero, which leads to the following equation:

$$\frac{1}{\eta} \cdot \frac{\partial p}{\partial x} = \frac{\partial^2 v_x}{\partial x^2}. \quad (9)$$

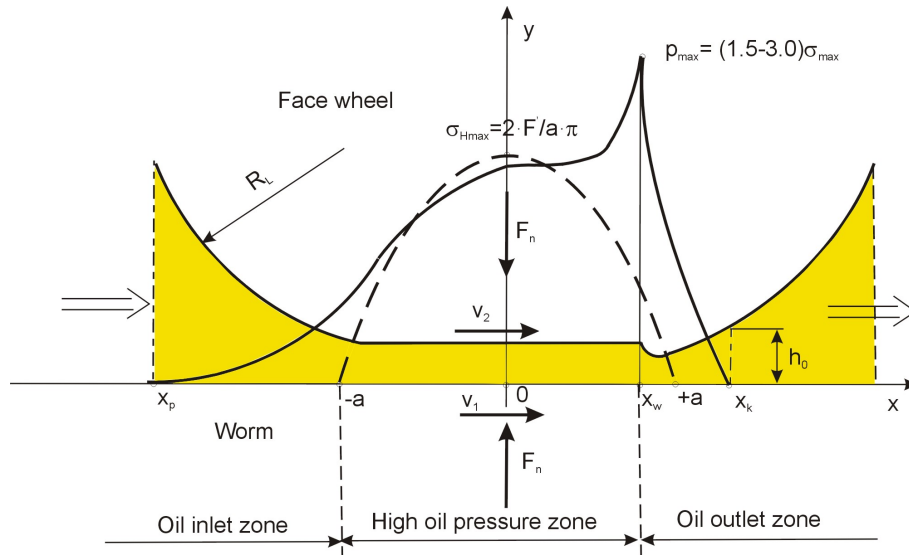


Fig. 6. Geometry, Hertzian stress and pressure distribution in the elastohydrodynamic oil film:  $\sigma_{Hmax}$  – maximum Hertzian stresses,  $p_{max}$  – maximum oil film pressure,  $R_L$  – radius of the face wheel tooth,  $v_{1,2}$  – linear speeds of the worm and face wheel surfaces

By integrating Equation (9) further, the following relation for the oil flow velocity in the tooth space is obtained:

$$v_x = \frac{1}{2} \cdot \frac{1}{\eta} \cdot \frac{\partial p}{\partial x} \cdot y^2 + C_1 \cdot y + C_2. \quad (10)$$

Constants  $C_1$  and  $C_2$  were determined from Equation (10) (Fig. 6) by assuming the following boundary conditions:

$$\begin{aligned} y = 0 &\rightarrow v_x = v_1 \\ y = h &\rightarrow v_x = v_2 \end{aligned} \quad (11)$$

The transformations of Equation (10) resulted in a function describing the velocity of the oil flowing through the tooth space and its derivative:

$$v_x = \frac{1}{2} \cdot \frac{1}{\eta} \cdot \frac{\partial p}{\partial x} \cdot (y^2 - h \cdot y) + \frac{y \cdot (v_2 - v_1)}{h} + v_1, \quad (12)$$

$$\frac{\partial v_x}{\partial x} = \frac{\partial}{\partial x} \left( \frac{1}{2} \cdot \frac{1}{\eta} \cdot \frac{\partial p}{\partial x} \cdot (y^2 - h \cdot y) + \frac{y \cdot (v_2 - v_1)}{h} + v_1 \right). \quad (13)$$

The equation of pressure distribution in the tooth space was obtained by inserting Equation (13) into the continuity equation for viscous and compressible fluids given by the following formula:

$$\text{div}(\rho \cdot v) = 0. \quad (14)$$

By integrating the oil flow continuity equation by the height of the tooth space  $y \in [0, h]$  in the adopted reference system,

$$0 = \int_0^h \frac{\partial}{\partial x} \left( \rho \cdot \frac{1}{2} \cdot \frac{1}{\eta} \cdot \frac{\partial p}{\partial x} \cdot (y^2 - h \cdot y) + \rho \cdot \frac{y \cdot (v_2 - v_1)}{h} + \rho \cdot v_1 \right), \quad (15)$$

the equation for the distribution of oil pressure in the tooth space was obtained:

$$\frac{\partial}{\partial x} \left( \rho \cdot h^3 \frac{\partial p}{\partial x} \right) = 12 \cdot \frac{\partial (h \cdot \rho)}{\partial x} \cdot \frac{v_1 + v_2}{2}. \quad (16)$$

## 5. PRESSURE DISTRIBUTION IN THE CONTACT ZONE BETWEEN THE WORM THREAD AND THE FACE WHEEL TEETH

The cooperation of the worm thread and the face wheel tooth was modelled as a linear contact between a cylinder and a plane. With this in mind, a function in the Cartesian coordinate system was adopted to describe the normal stress state  $\sigma_H(x)$  according to Hertz's theory:

$$\sigma_H(x) = \frac{\sigma_{H \max}}{a} \sqrt{a^2 - x^2}, \quad -a \leq x \leq a \quad (17)$$

where:  $a$  – width of the contact surface between the face wheel tooth and the work thread.

Assuming that the normal stress distribution along the contact surface does not change, the load related to the length of the contact line is  $F' = \frac{F}{b}$ , where  $b$  is the active length of contact.

For the contact of a cylinder and a plain, load  $F'$  is equal to half the area of an ellipse with conjugate radiuses  $\sigma_{H \max}, a$ :

$$F' = \sigma_{H \max} \cdot \frac{\pi \cdot a}{2}. \quad (18)$$

By transforming Equation (18), the maximum Hertzian stress can be described by the following formula:

$$\sigma_{H \max} = F' \cdot \frac{2}{\pi \cdot a}. \quad (19)$$

For a linear contact, the width of the contact surface is:

$$a = \sqrt{E_z \cdot F' \cdot R_L}, \quad (20)$$

where:  $R_L$  – face wheel tooth line radius [m]

$$E_z = \frac{1 - \nu_1^2}{E_1} + \frac{1 - \nu_2^2}{E_2} - \text{equivalent to Young's modulus, } \nu_{1,2} - \text{Poisson's number.} \quad (21)$$

## 6. CONTACT SURFACE DEFORMATION UNDER HIGH OIL PRESSURE

The space between the worm thread and the tooth of the face wheel into which the oil is supplied can be divided into three zones (Fig. 6): the inlet zone with low oil pressure, the Hertzian stress zone with high oil pressure and the outlet zone where the high-pressure oil flowing out is transported to the low-pressure zone.

Assuming that oil film height  $h$  is small in relation to the radius of the circular cylinder  $R_L$ , the shape of the slot in the zones where it does not deform can be represented as a contact between a parabolic cylinder and a half-plane:

$$h(x) = h_0 + \frac{x^2}{2 \cdot R_L} \quad (22)$$

In the high-pressure zone, surface deformations can be represented using the Flamant equation [24], which describes the effects of the normal force on an elastic half-space:

$$w(x) = -\frac{2 \cdot E_z}{\pi} \int_{-a}^a p(\xi) \cdot \ln(x - \xi) d\xi \quad (23)$$

## 7. CHARACTERISTICS OF THE OIL FILM IN THE CONTACT ZONE OF THE WORM AND THE FACE WHEEL

Equations (16–23) constitute a mathematical model of the isothermal elasto-hydrodynamic oil film generated in the mesh of the toothed rims of a spiroid gear. The literature offers different methods for solving the system of equations presented above. For a linear contact, the solution of the problem was presented, among others, by the authors of [25–30] in the form of a relation allowing for determining the minimum height of the oil film:

$$h_{min} = \frac{1,6 \cdot \alpha_p^{0,6} \cdot (\eta_0 \cdot u)^{0,7} \cdot E'^{0,03} \cdot \rho_z^{0,43}}{\left(\frac{F}{b}\right)^{0,13}} \quad (24)$$

where  $u = 0,5 \cdot (v_1 + v_2)$ . As a result of the study, Equation (24) was reduced to [25]:

$$h_{min} = \frac{2,65 \cdot \alpha_p^{0,54} \cdot (\eta_0 \cdot u)^{0,7} \cdot E'^{0,03} \cdot \rho_z^{0,43}}{\left(\frac{F}{b}\right)^{0,13}} \quad (25)$$

The formulas given by other researchers differ slightly in the values of the power exponents and the numerical value placed next to the piezo-viscosity coefficient  $\alpha_p$ .

In Equation (25), oil viscosity  $\eta_0$  is determined at the reference temperature  $T_0$ . As the results show, oil viscosity  $\eta_0$  is significantly influenced by its temperature  $T$  (Fig. 4). Therefore, a correction factor is introduced into the calculation of the minimum oil film height. In such cases, the non-isothermal oil film thickness is supplemented by the value of the correction factor  $C_{th}$  [25]. The correlation between the oil film height determined for the isothermal and non-isothermal model is represented by the relation:

$$\left(h_{min}\right)_{nis} = f\left(h_{min is}, C_{th}\right) \quad (26)$$

where  $C_{th}$  – a dimensionless factor correcting the effect of temperature on the minimum oil film height, nis – non-isothermal index, is – isothermal index, min – minimum.

This factor depends on the thermal conductivity of oil  $\lambda$ , oil viscosity  $\eta_0$  and the average speed of oil layers  $u$ . Its value can be determined using the following relation:

$$C_{th}(\xi) = \frac{1}{1 + 0,108 \cdot (\xi)^{0,62}} \quad (27)$$

The values of the dimensionless parameter  $\xi = \frac{u^2 \cdot \beta \cdot \eta_0}{\lambda}$  were determined for the dynamic viscosity model represented by the following equation:

$$\eta(p, T) = \eta_0 \cdot e^{\alpha_p \cdot p - \beta_T (T - T_0)}, \quad (28)$$

where:  $\alpha_p = \frac{1}{p} \cdot \ln \frac{\eta_p}{\eta_0}$  (29)

The piezo-coefficient of the effect of pressure on dynamic oil viscosity is given by:

$$\beta_T = \frac{\alpha_p \cdot p - \ln \frac{\eta_p}{\eta_0}}{T - T_0} \quad - \text{coefficient of the effect of temperature on oil viscosity} \quad (30)$$

A graphic presentation of Relation (27) is shown in Fig. 7.

When considering constructions, it is sometimes important to ensure elastohydrodynamic lubrication over a range of specific gear operating speeds. For such considerations, the permissible minimum oil film height guaranteeing the separation of the mating surfaces can be taken as a preset quantity. Its value can be assumed to depend on the roughness of the surface of the face wheel tooth and the worm thread  $R_{z1,2}$ . In the presented calculations, it was assumed that:

$$h_{lim} = 1.1(R_{z1} + R_{z2}) \quad (31)$$

By transforming Equation (25), the minimum angular velocity on the input shaft of the gear  $\omega_{1min}$  can be calculated from the following equation:

$$\pi \cdot \frac{n_{1min}}{30} = \omega_{1min} = \left( \frac{h_{lim}}{2.65 \cdot \alpha_p^{0.56} \cdot E^{0.03} \cdot \rho_z^{0.43} \cdot \left(\frac{F_n}{b}\right)^{-0.13}} \right)^{1.42857} \cdot \frac{1}{\eta_0 \cdot r_l}$$

where:  $\rho_z = \frac{1}{2 \cdot R_L}$  (32)

An analysis of Equation (32) shows that for a given contact geometry  $r_l$ ,  $\rho_z$ ,  $b$ , the minimum worm angular velocity  $\omega_{1min}$  guaranteeing elastohydrodynamic lubrication due to the power exponents mainly depends on the oil type  $\eta_0$ ,  $\alpha_p$  and toothed rim load  $F_n$ .

## 8. EFFECT OF OIL VISCOSITY GRADE ON GEAR LUBRICATION

Numerical calculations, including the determination of the input shaft rotational speed  $n_{1min} = \frac{\omega_{1min} \cdot 30}{\pi}$  at which elastohydrodynamic lubrication occurs, were carried out for preset quantities divided into the following three groups: Group 1 – quantities related to the geometry and materials of the worm and the face wheel, Group 2 – quantities related to the properties of the oil and Group 3 – related to the load on the gear. The preset quantities are shown in Table 1. Gear oils of VG according to standard [27], the properties of which are presented in Table 1, were adopted for this study. The classification was also supplemented with viscosity classes according to (AGMA Regular/EP) and SAE J306 (Table 2). Numerical calculations were used to obtain the minimum rotational speed of the input shaft  $n_{1min}$  for which the oil film of thickness  $h_{min} = h_{lim}$  was to be generated in the tooth space.

An analysis of the function graphs (Fig. 8) shows that the effect of the oil viscosity grade VG on rotational speed  $n_{1min}$  is significant. Thus:

- gears operating up to a worm rotational speed of  $n_l \leq 500$  rpm should be lubricated using gear oil with VG 220 or higher,

- in the speed range of  $n_l = 500-1,500$  rpm, the oil viscosity grade should be at least 100,
- the proper lubrication of gears operating at speed  $n_l > 2,500$  rpm is ensured by VG 46 oil.

The effect of normal force  $F_n$  occurring in the mesh of the worm and the face wheel on torque  $M_{t2}$  transmitted by the spiroid gear is shown in Fig. 9. Information on the method of determining the forces in the mesh between the face wheel and the worm is presented in the materials section [31].

An analysis of the literature on pinion gears showed certain discrepancies regarding the selection of oil viscosity grade (Table 3). The authors believe that the differences in the selection of oil viscosity grades may have resulted from the fact that the recommendations were developed for classic gears operating under average conditions. The calculations carried out by the authors present recommendations for the selection of oil viscosity grades for spiroid gears with design features defined by preset parameters.

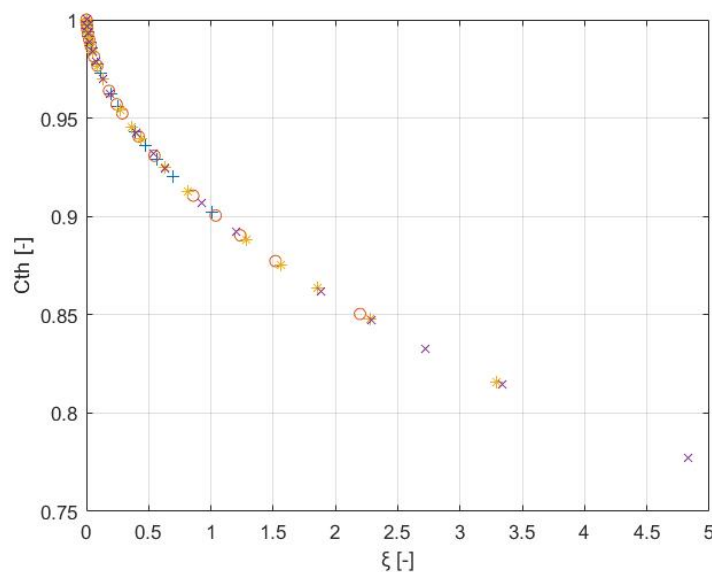


Fig. 7. Correction factor for the effect of temperature on minimum oil film height

## 9. DISCUSSION OF THE RESULTS

Ensuring a sufficiently high level of durability and reliability of a spiroid gear requires, among other things, selecting the appropriate type of oil, including its viscosity grade, to guarantee the generation of an elastohydrodynamic oil film between the worm thread and the face wheel teeth. This is a complex problem, as the height of the oil film is influenced not only by the type of oil but also by the mechanical properties of the worm and face wheel materials, relative speed, load, temperature and the geometry of the mating surfaces. As the results show, on the one hand, an increase in oil viscosity results in an increase in resistance to movement and, on the other hand, a lower rotational speed of the worm allows the mating surfaces to be separated by an oil film (Fig. 8).

It is also worth stressing the important relation between oil viscosity and meshing geometry. An increase in load results in a slight increase in the minimum speed at which the minimum oil film height is formed. These correlations are apparent from curves  $VG=f(R_L, b, F_n, n_l, \alpha, E_2)$  (Fig. 8). The recommendations presented in Table 3 can be used for the initial calculation of the operating parameters of a gear. However, in the case of verification calculations, the authors suggest using non-isothermal models to calculate the minimum worm speed to ensure fluid friction with elastohydrodynamic lubrication. The authors believe that the discussed calculations of non-isothermal oil films provided in Section 7 can improve the durability and reliability of spiroid gears.

In conclusion, the developed methodology for the selection of oil viscosity grade can be applied to initial calculations, as well as verification calculations for other types of gears.

In the next stage of their study, the authors will investigate the effects of oil viscosity tolerance and toothed rim geometric tolerance on gear lubrication conditions.

Table 1

## Preset quantities used in calculations

| Geometrical quantities |  |  |
|------------------------|--|--|
| $R_L$ [mm]             | Radius of face wheel tooth line  | $45.445 \cdot 10^{-3}$   |
| $r_1$ [mm]             | Pitch radius of worm thread  | $23.4 \cdot 10^{-3}$   |
| $b$ [mm]               | Length of contact surface between worm thread and face wheel tooth                                   | $4.14 \cdot 10^{-3}$   |
| $h_{lim}$ [mm]         | Permissible minimum oil film height  | $1.32 \cdot 10^{-6}$   |
| Young's modulus        |  |  |
| $E_1$ [Pa]             | Worm material  | $2.1 \cdot 10^{11}$  |
| $E_2$ [Pa]             | Face wheel material  | $2.1 \cdot 10^{11}$  |
| Poisson's number       |  |  |
| $\nu_1$ [-]            | Worm material  | 0.3  |
| $\nu_2$ [-]            | Face wheel material  | 0.3  |
| Properties of gear oil |  |  |
| $\eta_0$ [Pa·s]        | Dynamic viscosity at reference temperature and atmospheric pressure                                  | 0.198 (VG220)<br>0.135 (VG150)<br>0.090 (VG100)<br>0.0414 (VG46) |
| $\alpha_p$ [1/Pa]      | Pressure-dynamic viscosity piezo-coefficient   | $0.02 \cdot 10^{-6}$   |
| $\beta_T$ [1/°C]       | Temperature-dynamic viscosity coefficient  | $55.291 \cdot 10^{-3}$   |
| $\lambda$ [W/m·°C]     | Thermal conductivity of oil  | 0.145  |
| Gear load              |  |  |
| $F_n$ [N]              | Normal force applied to the contact surface and related to one tooth in contact with the worm thread | 10 - 10000   |

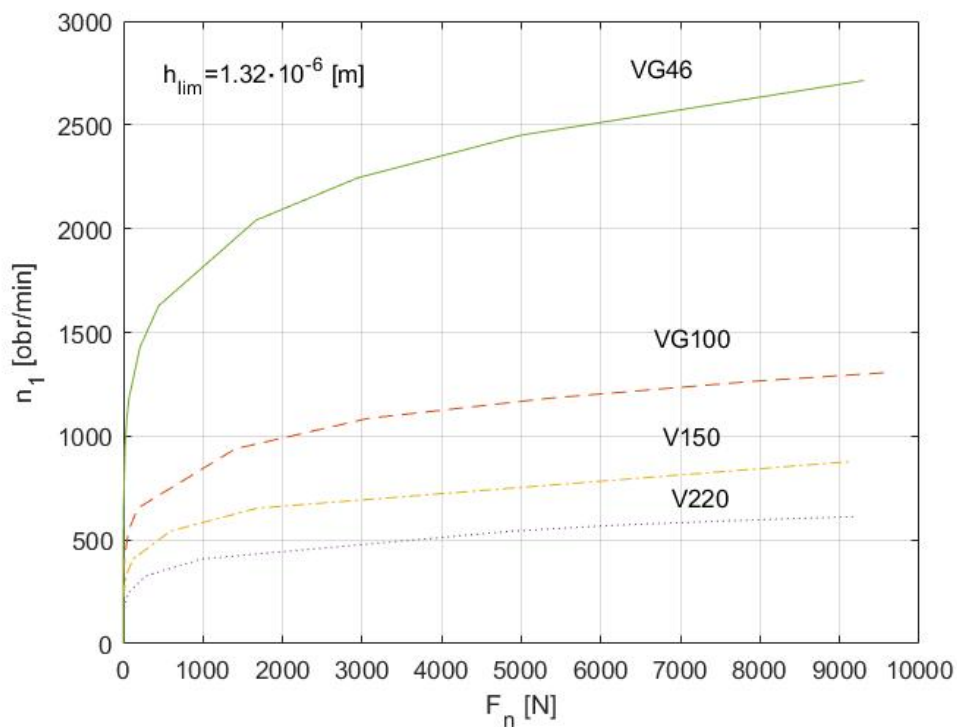


Fig. 8. Effect of the oil viscosity grade VG and the normal force  $F_n$  on the rotational speed  $n_1$  allowing the mating surfaces to be separated by an oil film of thickness  $h_{lim}$

Table 2

Viscosity grades of gear oils [32]

| ISO 3448 VG | Viscosity tolerance according to ISO 3448 | AGMA Regular/EP | SAE J306 |
|-------------|---|-----------------|----------|
| 46          | ±10%                                      | 1               | 75 W     |
| 100         |   | 3/3EP           | -        |
| 150         |   | 4/4EP           | 80W/90   |
| 220         |   | 5/5EP           | 90       |

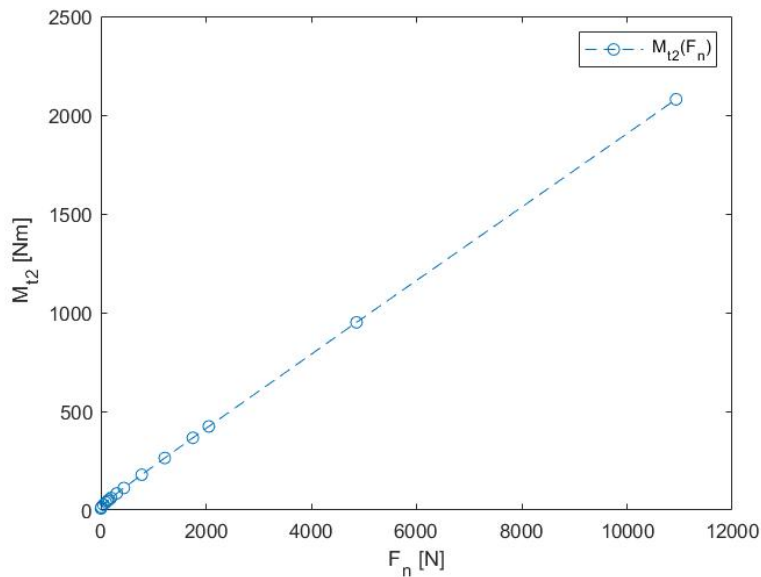


Fig. 9. Relation between normal force  $F_n$  and torque  $M_{t2}$

Table 3

Recommended oil viscosity grades for gears

| Own calculations                |   |                        | Dziama A. [33]                                    | Mueller L. [34]                                   |
|---------------------------------|---|------------------------|---|---|
| Worm rotational speed $n_1$ rpm | Linear velocity at the outer diameter of worm $v_1$ m/s | Oil viscosity grade VG | $v_1$ m/s/ oil viscosity $\text{mm}^2/\text{s}^2$ | $v_1$ m/s/ oil viscosity $\text{mm}^2/\text{s}^2$ |
| Up to 500                       | Up to 1.3   | 220 (124)*             | 1/114*  | 1/(180–300)*                                      |
| 500–1,000                       | 1.3–2.7   | 150 (87)*              | 2.5/80*   | 2.5/(125–200)*                                    |
| 1,000–1,500                     | 2.7–4.0   | 100 (60)*              | 5/59*   | 4/(100–160)*                                      |
| 1,500–2,500                     | 4.0–6.6   | 46 (30)*               | 12.5/43*  | 10/(70–100)*                                      |

\*viscosity at 50°C

**References**

1. Żabicki, M. Diagnostyka przekładni zębatych - Diagnostyka, Pomiary, Regulacja. *Główny Mechanik*. January-February, 2020. [In Polish: Gearbox Diagnostics - Diagnostics, Measurements, Adjustments. *Chief Mechanic*].
2. Lawrowski, Z. *Tribologia, tarcie, zużycie, i smarowanie*. PWN Scientific Publishing House. Warsaw, 1993. [In Polish: *Tribology, Friction, Wear, and Lubrication*].
3. Hebda, M. & Wachal, A. *Trybologia*. WNT. Warsaw, 1980. [In Polish: *Tribology*].
4. Chodoła, Ł. & Mazurkow, A. & Surowaniec, M. & Markowski, T. & Homik, W. Measurement method of temperature of the face gear rim of a spiroid gear. *Sensor an Open Access Journal by MPDI*. 2022. Vol. 22. No. 22.

5. Davall. Available at: <https://www.davall.co.uk/>.
6. Spiroid. Available at: <https://www.spiroidgearing.com/application-industries>.
7. Trubachev, E. Spiroid gears as an alternative to bevel and hypoid gears. In: *Proceedings of the 9th International Conference on Industrial Engineering (ICIE 2023)*. 2023. P. 71-82.
8. Litvin, F.L. & Nava, A. & Qi Fan, Fuentes A. New geometry of worm face gear drives with conical and cylindrical worms: generation, simulation of meshing, and stress analysis. *NASA/CR-2002-211895 ARL-CR-0511 U.S. Army Research Laboratory*. University of Illinois at Chicago. Chicago, Illinois. November, 2002.
9. Trubachev, E.S. & Kuznetsov, A.S. & Sannikov, A.M. *Advanced Gear Engineering*. MMS 51. Springer. P. 45-72. 2018.
10. Goldfarb, V.I. What we know about spiroid gearing. In: *Proceedings of the International Conference on Mechanical Transmissions*. 2006. Vol. 1. P. 19-26.
11. Abadjiev, V. & Abadjieva, E. On approach to the synthesis, design and manufacture of hyperboloid gear sets with face mating gears. Part 1: Basic theoretical and CAD experience. *Journal of Theoretical and Applied Mechanics*. 2016. Vol. 46. No. 2. P. 3-26.
12. Goldfarb, V. & Trubachev, E. & Barmina, N. Innovations in design and production of spiroid gears in the XXI century. In: *MATEC Web of Conferences. Power Transmissions*. 2019. Vol. 287. No. 01002.
13. Frąckowiak, P. Ślad zazębienia w płaskiej przekładni spiroidalnej. *Archiwum Technologii Maszyn i Automatyzacji*. 2009. Vol. 19. No. 4. P. 59-71. [In Polish: Mesh pattern in a flat spiroid gear].
14. Total. Available at: <https://totalenergies.pl>.
15. Belicke, R. & Bobach, L. & Bader, N. & Poll, G. & Brouwer, L. & Schwarze, H. Tribologische Fluid Modelle Zur Simulation der Reibung in geschmiertenkonzebrierten Kontakte. In *Tribologie – Fachtagung, Gesellschaft fuer Tribologie*. V. Getynga. 2015. [In German: Tribological fluid models for simulating friction in lubricated concentrated contacts. In: *Tribology – specialist conference, Society for Tribology*].
16. Spalek, J. & Kwaśny, M. Diagnostyczna weryfikacja wpływu lepkości oleju smarującego na pracę przekładni zębatej. *Szybkobieżne Pojazdy Gąsienicowe*. 2012. Vol. 29. No. 1. [In Polish: Diagnostic verification of the influence of lubricating oil viscosity on the operation of the gear train. *High-speed Tracked Vehicles*].
17. Rodermund, H. Extrapolierende Berechnung des Viskositaetsverlaufsunterhohen Drucken. *Schmiertechnik + Tribologie*. 1981. Vol. 27. No. 4. P. 3-5. [In German: Extrapolating calculation of the viscosity curve under high pressure. *Lubrication technology + tribology*].
18. Kuss, E. Die Bedeutung der Viskositaets – druck- abhaendigkeit in der klassischen und der elastohydrodynamischen Theorie der Schmierung. [In German: The importance of viscosity-pressure dependence in the classical and elastohydrodynamic theory of lubrication]. *Mineraloeltechnik*. 1973. Vol. 18. P. 1-48.
19. Baru, C. Isothermals, isopiestic and isometric relative to viscosity. *American Journal of Science*. 1893. Vol. 45. P. 87-96.
20. Buković, A. & Gajecić, S. & Skulić, A. & Savić, S. & Ašonja, A. & Stojanović, B. Tribological application of nanocomposite additives in industrial oils. *Lubricants*. 2024. Vol. 12. No. 6. DOI: 10.3390/lubricants12010006.
21. Skulić, A. & Milojević, S. & Marić, D. & Ivanović, L. & Krstić, B. & Radojković, M. & Stojanović, B. The impact of lubricant viscosity and materials on power losses and efficiency of worm gearbox. *Tehnički vjesnik*. 2022. Vol. 29(6). P. 1853-1860. DOI: 10.17559/TV-20220207092015.
22. Krzemiński-Freda, H. *Rozkład ciśnienia i kształt filmu olejowego przy współpracy elementów tocznych smarowanych elastohydrodynamicznie*. Rozprawa doktorska. Łódź. 1969. [In Polish: Pressure distribution and oil film shape during the cooperation of elastohydrodynamically lubricated rolling elements. *Doctoral dissertation*].
23. Schouten, M.J.W. *Theoretische und experimentelle Untersuchungen Zur Erweiterung der EHD – Theorie auf praxisnahe und instationaere Bedigungen*. Frankfurt. FKM – Heft. Maschinenbau Verlag. 1978. No. 72. [In German: *Theoretical and experimental investigations to extend the EHD theory to practical and unsteady conditions*].

24. Paluch, M. *Teoria sprężystości*. Krakow University of Technology Publishing House 2006. Krakow. [In Polish: Theory of Elasticity].
25. Haddad, N. *Viskositäts – und Reibungsmessungen im EHD – Linienkontakt*. Diss. TU Hannover. 1985. [In German: *Viscosity and friction measurements in EHD line contact*].
26. Rodermund, H. *Beitrag Zur Elastohydrodynamischen Schmierung Von Evolventenzahnredern*. Diss. TU Clausthal. 1975. [In German: *Contribution to elastohydrodynamic lubrication of involute toothed gears*].
27. Evertz, F. & Gangireddy, M. & Mork, B. & Porter, T. & Quist, A. High Torque Skew Axis Gearing – Technical Primer. *Spiroid High Torque Gearing*. 2021. P. 1-19. Available at: [https://www.spiroidgearing.com/wp-content/uploads/2019/05/Spiroid-Technical-Paper\\_Final.pdf](https://www.spiroidgearing.com/wp-content/uploads/2019/05/Spiroid-Technical-Paper_Final.pdf)
28. Dowson, D. & Higginson, G.R. A numerical solution to the elasto-hydrodynamic problem. *J. Mech. Engng. Sci.* 1959. Vol. 1. P. 6-15.
29. Ivanović, L. & Josifović, D. & Ilić, A. & Stojanović, B. Tribological aspect of the kinematical analysis at trochoidal gearing in contact. *Journal of the Balkan Tribological Association*. 2011. Vol. 17. No. 1. P. 37-47.
30. Tomović, R. & Ivanović, L. & Mačkić, T. & Stojanović, B. & Glišović, J. Prediction of oil film thickness in trochoidal pump. *Transactions of the Canadian Society for Mechanical Engineering*. 2021. Vol. 45. No. 3. P. 374-385. DOI: 10.1139/tcsme-2020-0105.
31. Mazurkow, A. *Analiza obciążeń przekładni spiroidalnej*. [In Polish: *Analysis of Spiroid Gear Loads*]. Materials of the Department of Machine Design. Rzeszow University of Technology. 2021.
32. PN-ISO 3448:2009. *Klasyfikacja lepkościowa olejów*. Warsaw: Polish Committee for Standardization. [In Polish: *Viscosity classification of oils*].
33. Dziama, A. & Michniewicz, M. & Niedźwiedzki, A. *Przekładnie zębate*. Scientific Publishing House PWN. 1995. [In Polish: *Gears*].
34. Mueller, L. *Przekładnie zębate. Projektowanie*. Scientific Technical Publishing House. 1995. [In Polish: *Gears. Design*].

Received 13.02.2023; accepted in revised form 05.09.2024